2006

Reductive biotransformation of Fe in shale–limestone saprolite containing Fe(III) oxides and Fe(II)/Fe(III) phyllosilicates

Ravi K. Kukkadapu
Pacific Northwest National Laboratory, ravi.kukkadapu@pnl.gov

John M. Zachara
Pacific Northwest National Laboratory, john.zachara@pnl.gov

James K. Fredrickson
Pacific Northwest National Laboratory, jim.fredrickson@pnl.gov

James P. McKinley
Pacific Northwest National Laboratory

David W. Kennedy
Pacific Northwest National Laboratory

See next page for additional authors

Available online at www.sciencedirect.com
SCIENCE DIRECT
Geochimica et Cosmochimica Acta 70 (2006) 3662–3676
Geochimica
www.elsevier.com/locate/gca

Reductive biotransformation of Fe in shale–limestone saprolite containing Fe(III) oxides and Fe(II)/Fe(III) phyllosilicates

Ravi K. Kukkadapu [a,*], John M. Zachara [a], James K. Fredrickson [a], James P. McKinley [a], David W. Kennedy [a], Steven C. Smith [a], Hailiang Dong [b]

[a] *Pacific Northwest National Laboratory, P.O. Box 999, MSIN K8-96, Richland, WA 99354, USA*
[b] *Department of Geology, Miami University, Oxford, OH 45046, USA*

Received 10 August 2005; accepted in revised form 3 May 2006

Abstract

A <2.0-mm fraction of a mineralogically complex subsurface sediment containing goethite and Fe(II)/Fe(III) phyllosilicates was incubated with *Shewanella putrefaciens* (strain CN32) and lactate at circumneutral pH under anoxic conditions to investigate electron acceptor preference and the nature of the resulting biogenic Fe(II) fraction. Anthraquinone-2,6-disulfonate (AQDS), an electron shuttle, was included in select treatments to enhance bioreduction and subsequent biomineralization. The sediment was highly aggregated and contained two distinct clast populations: (i) a highly weathered one with "sponge-like" internal porosity, large mineral crystallites, and Fe-containing micas, and (ii) a dense, compact one with fine-textured Fe-containing illite and nano-sized goethite, as revealed by various forms of electron microscopic analyses. Approximately 10–15% of the $Fe(III)_{TOT}$ was bioreduced by CN32 over 60 d in media without AQDS, whereas 24% and 35% of the $Fe(III)_{TOT}$ was bioreduced by CN32 after 40 and 95 d in media with AQDS. Little or no Fe^{2+}, Mn, Si, Al, and Mg were evident in aqueous filtrates after reductive incubation. Mössbauer measurements on the bioreduced sediments indicated that both goethite and phyllosilicate Fe(III) were partly reduced without bacterial preference. Goethite was more extensively reduced in the presence of AQDS whereas phyllosilicate Fe(III) reduction was not influenced by AQDS. Biogenic Fe(II) resulting from phyllosilicate Fe(III) reduction remained in a layer-silicate environment that displayed enhanced solubility in weak acid. The mineralogic nature of the goethite biotransformation product was not determined. Chemical and cryogenic Mössbauer measurements, however, indicated that the transformation product was not siderite, green rust, magnetite, $Fe(OH)_2$, or Fe(II) adsorbed on phyllosilicate or bacterial surfaces. Several lines of evidence suggested that biogenic Fe(II) existed as surface associated phase on the residual goethite, and/or as a Fe(II)–Al coprecipitate. Sediment aggregation and mineral physical and/or chemical factors were demonstrated to play a major role on the nature and location of the biotransformation reaction and its products.

1. Introduction

Bacterial iron reduction is an important process in anoxic soils, sediments, and subsurface materials. This critical aspect of the iron biogeochemical cycle is driven, to large degree, by the activities of dissimilatory metal-reducing bacteria (DMRB; Lovley, 1991, 1993; Nealson and Saffarini, 1994). DMRB are capable of using solid-phase Fe(III) in both oxide (e.g., ferrihydrite, goethite) and phyllosilicate (e.g., montmorillonite, illite) form as an electron acceptor for respiration. These two forms of Fe(III) often predominate in the reactive, high surface area, clay-sized fraction of oxidized soils and subsurface materials. The bioavailability of mineral Fe(III) to metal-reducing bacteria appears limited by numerous incompletely understood factors, such as crystal chemistry, solid-phase thermodynamics and surface area, and electron transfer efficiency at the mineral–microbe interface.

Dissimilatory bacterial reduction of Fe(III) oxides and associated mineral transformations have been well studied in single-phase Fe(III)-oxide suspensions (e.g., Roden and

* Corresponding author. Fax: +1 509 376 3650.
E-mail address: ravi.kukkadapu@pnl.gov (R.K. Kukkadapu).

0016-7037/$ - see front matter © 2006 Elsevier Inc. All rights reserved.
doi:10.1016/j.gca.2006.05.004

Zachara, 1996; Fredrickson et al., 1998, 2001; Zachara et al., 1998, 2002; Nevin and Lovley, 2000; Kukkadapu et al., 2004, 2005; Roden, 2004), and the general factors that control the reduction rate, the extent of reduction, and the distribution of reduction products are known. Comparable information on Fe(III)-containing phyllosilicates is limited, making generalizations more difficult (e.g., Kostka et al., 1996, 1999; Favre et al., 2002). Experiments with single-phase suspensions indicate that phyllosilicate reactivity is variable. Significant quantities (9–90%) of octahedral Fe(III) in high-surface area, clay-sized ferruginous smectite and montmorillonite were rapidly reduced by *S. putrefaciens*, strain MR-1, in dilute anoxic suspensions (Kostka et al., 1996, 1999). The reduction rate and the extent in this system decreased with increasing suspension density (Kostka et al., 1996). In contrast, only a small fraction of octahedral Fe(III) in clay-sized illites (a non-swelling phyllosilicate) were reduced by *S. putrefaciens*, strain CN32 (a functionally similar organism to MR-1) unless an electron shuttle, anthraquinone-2,6-disulfonate (AQDS), was added to facilitate electron transfer to the solid phase (Dong et al., 2003; Seabaugh et al., 2006).

The bacterial reduction of Fe(III)-oxides produces a biogeochemically active pool of Fe that includes Fe^{2+}_{aq}, Fe(II) adsorption complexes on mineral surfaces, and mineral Fe(II) (e.g., siderite). These Fe forms may be reactive with polyvalent metals such as chromate ($Cr(VI)O_4^{2-}$; Loyaux-Lawniczak et al., 2000; Williams and Scherer, 2001), the uranyl ion [$U(VI)O_2^{2+}$] and its complexes (Liger et al., 1999; Fredrickson et al., 2000; O'Loughlin et al., 2003; Jeon et al., 2004), pertechnetate [$Tc(VII)O_4^-$; Fredrickson et al., 2004], and with organic contaminants (e.g., Haderlein and Pecher, 1998; Amonette et al., 2000; Pecher et al., 2002; Williams et al., 2005). The bacterial reduction of phyllosilicate Fe(III), on the other hand, yields structural Fe(II) and/or adsorption and ion exchange complexes on the residual layer silicate (e.g., Jaisi et al., 2005). These biogenic Fe(II) forms may also be reactive towards organic contaminants (e.g., Cervini-Silva et al., 2001; Hofstetter et al., 2006).

The bioreductive transformations of Fe(III)-containing minerals and the identity of biogenically produced Fe(II) in composite mineral material are not well understood because of the difficulty in characterizing the low concentrations of labile Fe that typically exist in natural materials. Curiously, the few reported studies of the mineralogic impacts of bacterial iron reduction in subsurface sediments (Kukkadapu et al., 2001; Zachara et al., 2004; Cooper et al., 2005) have shown that the effects are small, and the degrees of biotransformation and biomineralization are different from those expected based on single-phase mineralogic studies (i.e., those with just phyllosilicates or Fe(III) oxides; Kostka et al., 1999; Zachara et al., 2002; Jaisi et al., 2005). These differences may result from the associated mineral fraction and sediment aggregation that mediate reactions and effects that would not occur in their absence. Unresolved is whether oxide Fe(III) and phyllosilicate Fe(III) in soil and subsurface sediments compete for electron equivalents liberated by microbial respiration. Does such competition occur, and which of these electron acceptors is preferentially reduced by bacteria in a dilute mixture of these phases with other mineral components?

In this communication, we investigate the bacterial transformations of Fe(III) in a shale–limestone saprolite of complex mineralogy (various pools of Fe; complex mineral association and micro-structures, etc) that was incubated with a DMRB and an electron donor under anoxic conditions. The sediment was obtained from a field site where bacterial Fe(III) reduction is being investigated as a potential remedial technique to arrest the subsurface migration of mobile U(VI) and Tc(VII) (e.g., Istok et al., 2004; North et al., 2004). Goethite and phyllosilicates were the primary Fe(III) containing mineral phases in the sediment. Laboratory investigations were performed to identify: (i) which of these phases were the preferred electron acceptor for bacterial Fe(III) respiration, (ii) the chemical and physical reasons for preference if observed, and (iii) the mineralogic nature of the biogenic Fe(II) reaction products. Anthraquinone disulfonate (AQDS) was used in select treatments to enhance bacterial reduction to facilitate in bioproduct identification. We have previously shown (Fredrickson et al., 2004) that the bioreduction of this sediment, yields "sorbed" Fe(II) that reduces $Tc(VII)O_4^-$, and that exhibits an Fe(II) paramagnetic doublet in its 77 K Mössbauer spectrum that was not well-resolved from phyllosilicate Fe(II). Here we strive to identify the nature of this biogenic Fe(II) product, and the Fe(III) containing mineral phases from which they were derived using chemical extractions, transmission electron microscopy and electron microprobe, and variable-temperature Mössbauer spectroscopy.

2. Materials and methods

2.1. FRC sediment

The subsurface sediment (background sediment; SB002-03-002) was obtained from a U.S. Department of Energy experimental site (Oak Ridge Field Research Center) where in situ stimulation of bacterial activity is being studied as a potential approach to arrest the subsurface migration of mobile radionuclide contaminants (http://www.lbl.gov/nabir). The sediment was provided by David Watson (Oak Ridge National Laboratory). Iron reducing bacteria exist in these sediments and associated groundwaters that can be stimulated in the field by additions of ethanol (North et al., 2004; Peacock et al., 2004).

Extractable Fe(III)-oxides were determined using methods as previously described (Zachara et al., 1998), including acidified ammonium oxalate (AAO; Schwertmann, 1959) for poorly crystalline oxides, and dithionite–citrate–bicarbonate (DCB; Mehra and Jackson, 1960) for reducible Fe(III) oxides. Weak acid (0.5 N HCl) extraction was used to determine the "biovailable Fe(III) oxide"

content (ferrihydrite primarily) of the sediment (Anderson et al., 1998). After chemical extractions, the filtrates were analyzed for [Fe(II)] and [Fe_{TOT}] using the ferrozine assay (Lovley and Phillips, 1986; Stookey, 1970) and the residues analyzed by Mössbauer spectroscopy.

2.2. Acid treatment of DCB-reduced FRC sediment

The FRC sediment was treated with DCB reagent twice at room temperature (RT) with stirring for 2 d (15 g FRC/150 mL DCB reagent). The treated sediment was centrifuged (5000 relative centrifugal force for 30 min), the centrifugate decanted, and the solids resuspended in 125 mL $CaCl_2{\cdot}2H_2O$ (0.5 M) for 24 h to remove ion-exchangeable Fe(II). The $CaCl_2{\cdot}2H_2O$ was decanted after centrifugation and the sediment was washed four times with 150 mL of 30 mM, pH 7, 1,4-piperazinediethanesulfonic acid (PIPES) buffer. The sediment was then treated with small volume of 1 N HCl (to pH 4.5) to ensure that no precipitated calcium carbonate existed in the suspension. The sediment was resuspended and stored in PIPES buffer after acid treatment.

The acid-dissolution of the DCB-reduced, $CaCl_2{\cdot}2H_2O$-treated FRC sediment was studied by suspending 0.2 mL of the pH 7 suspension (1 g/10 mL suspension) in 3.8 mL of 0.53 N HCl. Each treatment and sampling event was replicated three times, and separate tubes were sacrificed at each time-point (1 min to 7 d) for chemical analysis. Supernatants from the centrifuged suspensions were analyzed for [Fe(II)] by the ferrozine assay, and for [Fe_{TOT}], [Si], and [Al] by inductively-coupled plasma spectroscopy (ICP).

2.3. Bacteria and media

Shewanella putrefaciens strain CN32 was isolated from a subsurface core sample (250 m beneath the surface) in northwestern New Mexico (Fredrickson et al., 1998). Stock cultures were maintained by freezing in 40% glycerol at −80 °C. CN32 was cultured aerobically in tryptic soy broth (TSB), 27 g L^{-1} (Difco Laboratories, Detroit, MI). CN32 cells were harvested from TSB cultures at mid to late log phase and were separated by centrifugation and washed twice with 30 mM, pH 7, PIPES buffer to remove residual medium, and once with the final buffer (PIPES or 30 mM sodium bicarbonate). Cells were resuspended in bicarbonate or PIPES buffer and purged with O_2-free N_2:CO_2 (80:20) or N_2, respectively.

2.4. Bacterial reduction experiments

Bioreduced sediments were generated by incubating 1 g of the <2.0 mm sediment in 10 mL of 30 mM, pH 7, buffer (30 °C) with 8×10^7 cells/mL. Sodium lactate (10 mM) was added as an electron donor and headspace gas was adjusted depending on buffer: N_2:CO_2 (80:20) (for bicarbonate-buffered medium) or N_2 (for PIPES-buffered medium). AQDS (0.1 mM) was included in the media of select treatments. The tubes were shaken horizontally at 25 rpm. Each treatment and sampling event was replicated three times, and separate tubes were sacrificed at each time-point for chemical analyses. At select time points, samples from one of the replicate tubes were withdrawn for powder XRD and Mössbauer spectroscopy measurements. Abiotic controls consisted of suspensions that received 1 mL of anaerobic buffer in place of the CN32 cell suspension.

2.5. Chemical analyses of bioreduced sediments

Replicate tubes containing controls and bioreduced suspensions were transferred to an anaerobic (Ar:H_2, 95:5) glove bag (Coy Laboratory Products, Inc., Grass Lake, MI) and allowed to settle for 1 h. The tubes were opened, and 1 mL of clear solution was removed. The subsample (0.5 mL) was filtered (0.2 μm) into 0.5 mL of 1 N HCl in a polystyrene tube. This fraction was considered to be the aqueous fraction. Acid-extractable components (0.5 N HCl) were obtained by adding 9 mL of 1 N HCl to the remaining 9 mL of sample, and shaking at 25 rpm for 1 h. A calcium chloride extraction was performed by adding 0.5 M $CaCl_2{\cdot}2H_2O$ to a sub-sample of the sediment that had been incubated with CN32 in PIPES buffer (60 d), and shaken at RT for 2 h. The equilibrated extracts were filtered through 0.2-μm polycarbonate syringe filters. The aqueous, weak-acid extractable, and exchangeable fractions were analyzed for Fe(II) and Fe_{TOT} using the ferrozine assay, and for Mn and Fe_{TOT} by ICP.

2.6. Backscattered electron imaging (BSE)/Electron microprobe analysis (EMP)

Mineral particles were imbedded in epoxy resin ('EpoThin', Buehler, Irvine, CA), then cut and polished on a glass slide. The petrographic thin sections were examined using a JEOL 8200 electron microprobe to determine the aggregate/physical structure of the fundamental sediment particles, their relative porosity, and the physical locations and semi-quantitative composition of fine-grained Fe-containing mineral particles. BSE of microscale atomic-number contrast was used to examine the qualitative variability in clast textures, morphologies and compositions.

For elemental abundance maps, crystal spectrometers were tuned to the characteristic X-ray emission lines for Fe and K, and the sample was moved at 2 μm steps under the focused, <1 μm diameter beam of 20 keV electrons with a current of 20 nA and a single-point dwell time of 100 ms. The mapped concentrations were calculated as simple K-ratio proportions against X-ray fluxes from mineral standards (SPI, West Chester, PA); the abundances were not corrected for inter-element effects. For mineral-specific compositional analyses, the instrument was calibrated against mineral standards and raw X-ray counts were reduced using an atomic number-absorption-fluorescence

routine included in instrument automation software. Representative mica clasts were grouped according to similarities in elemental abundances (e.g., low-K high-Fe, and high-Fe low-K micas were distinguished qualitatively), morphology, and texture. For comparison, previously grouped compositions were averaged, and then reduced to mica structural formulae. The calculations were constrained by normalizing the cation equivalents to a total anion charge of −44 (22 oxygens), and specifying that the cation tetrahedral occupancy be equal to 8.

2.7. ^{57}Fe Mössbauer spectroscopy

Mössbauer analysis of the pristine sediment was performed on air-dried samples, while those of bioreduced sediments were performed on suspension subsamples that were filtered, washed, and dried in an anoxic chamber (Kukkadapu et al., 2004). Details of the Mössbauer instrumentation and sample preparation procedure were reported by Kukkadapu et al. (2004). The prepared Mössbauer disks of the bioreduced sediments were stored at −80 °C in an anoxic chamber until analysis. A closed-cycle cryostat (ARS, Allentown) was employed for low temperature measurements.

The Mössbauer data were modeled with the *Recoil* software using a Voigt-based spectral fitting routine (Rancourt and Ping, 1991). In the Voigt-based method, each distribution [quadrupole splitting distribution (QSD) and hyperfine field distribution (HFD)] is represented by a sum of Gaussians having different positions, widths, and relative areas. The number of Gaussians used for a given fit was the minimum required for good statistics. The coefficients of variation of the spectral areas of the individual sites generally ranged between 1% and 2% of the fitted value. The following guidelines were used in the modeling of the Mössbauer data: (i) all doublets were assumed to be symmetric, (ii) for sextets, the ratios of the spectral areas of peak 1 to peak 3, and peak 2 to peak 3 were fixed at 3 and 2, respectively, (iii) coupling was not allowed between δ (isomer shift) or the CS (center shift) with the distributed hyperfine parameter [quadrupole splitting (Δ or QS)], and (iv) coupling was not allowed between the quadrupole shift parameter (ε) and the distributed hyperfine parameter (z).

3. Results

3.1. Properties of the background saprolitic sediment

3.1.1. Mineralogy

The <2.0-mm fraction contained 4.4 wt% of Fe per gram of sediment, as determined by XRF analysis. Approximately 40% of the total Fe (Fe_{TOT}) was extracted by DCB. Only a small amount of the DCB-extractable Fe(III) could be extracted by AAO, indicating that most of the reducible Fe(III) oxides were crystalline (Fredrickson et al., 2004). Poorly crystalline Fe(III)-oxides (e.g., ferrihydrite) dissolve quickly in AAO (Schwertmann, 1959; Schwertmann and Fischer, 1973).

Peaks due to discrete Fe(III)-oxides (e.g., goethite) were absent in the XRD pattern (not shown). Quartz dominated the spectrum (~70%), whereas illite/muscovite, Fe-vermiculite (Moore and Reynolds, 1997), and quartz were dominant in the <2-μm fraction that was Mg^{2+} saturated and subsequently treated with glycerol. K^{+} saturation and 110 °C heat treatment indicated that vermiculite layers were partially filled with hydroxy-Al species (Barnhisel and Bertsch, 1989).

Transmission electron microscopy analyses of the <2-μm fraction (not shown) revealed the presence of: (i) common lath-shaped crystals of goethite twinned to yield "star-shaped" composites, as well as more abundant discrete laths without twinning, and (ii) abundant illite. "Star-shaped" goethite composites were far less abundant in the <2.0-mm fraction. Energy-dispersive X-ray analysis of the goethite crystallites indicated partial Al substitution (15–20%). The illite crystals were plate-shaped, and their corresponding selected area electron diffraction pattern was typical of a 1-Md pattern.

3.1.2. Aggregate structures and Fe spatial distribution

Backscattered electron imaging (BSE) of sediment thin sections (Fig. 1a) showed that the sediment consisted of millimeter-sized clasts comprised of aggregates of smaller crystalline materials. Moreover, two distinct clast types were recognizable: (i) weathered darker-grey ones containing larger crystallites and significant, "sponge-like" internal pore space, and (ii) lighter-grey, compact ones with very small crystallites, limited internal porosity, and occasional "bedding-plane like" microfractures (Fig. 1b). The two clast groupings were clearly heterogeneous at the millimeter scale and below.

Electron microprobe analyses (EMP) were performed to identify the distribution and mineralogic residence of Fe, particularly for the phyllosilicate fraction. The weathered clasts consisted of an interlocking porous matrix of ca. 50 μm quartz crystallites (uniform mid-grey particles) embedded with other minor mineral phases defined by K and Fe distributions (Fig. 1b). The high K regions (red-magenta) with spherical/oblong morphology were shown to be feldspars by these and other analyses. Other areas of K localization correlated exactly with Fe, defining different populations of blade-like crystallites discriminated by Fe concentration (e.g., high—green and low—dark blue). EMP analyses of these regions (not shown) defined them to be micas of two primary types: (i) high Fe and low K, and (ii) low Fe and high K.

The compact clast was comprised of a fine groundmass containing qualitatively equal K and Fe concentrations (~5%). EMP of this ground mass (16 distinct point analyses) were consistent with Fe-containing illite (not shown). Discontinuous, infrequent pore space was evident as 5-10 μm black regions in the Fe and K images. Imbedded in the illite groundmass were a variety of minor phases

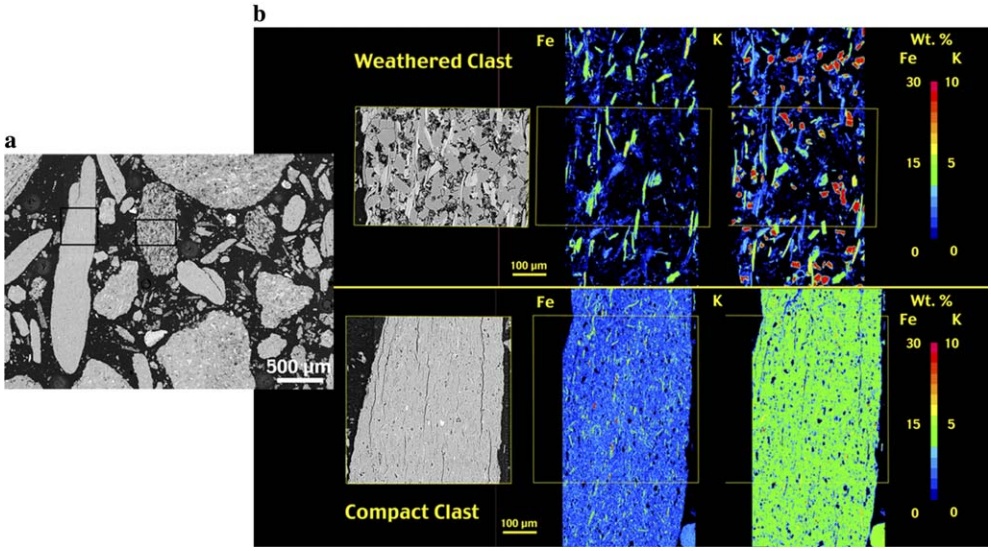

Fig. 1. (a) Backscattered electron micrograph of an FRC sediment thin section showing a typical distribution of aggregates and grain sizes. Two different clast types were always observed: weathered (darker grey) and compact (lighter grey). (b) Electron microprobe element abundance maps for Fe and K in weathered and compact clast domains noted in (a).

including Fe(III) oxides (small red spots in Fe image) and micas (green blades in the Fe image). Four microprobe analyses were performed of the imbedded micas; these were 1 μm wide and difficult to isolate analytically. These micas also contained appreciable Fe and were compositionally intermediate to the two types found in the weathered clast (not shown). Zones of vermiculite and hydroxy-Al-interlayer vermiculite (HIV) were insufficiently delineated by morphology or chemical signature in either clast, possibly because of small size, to allow their defensible analysis by EMP.

The elemental abundance maps were converted to normalized trilateral plots of Fe, Si, and K atomic abundances (not shown). The results provided an estimate of the qualitative differences between compact and weathered clasts. For the weathered clast, more than 80% of the total analyses had a normalized atomic Fe concentration of less than 10%, and the average Fe for the map was 2.12 wt%. The clast overall was poor in Fe. For the compact clast, 70% of the total analyses defined an area within the plot that ranged in normalized atomic Fe concentration from about 5–15%, and the average Fe for the map was 6.12 wt%. The clast overall included significant Fe.

3.1.3. Fe valence and phase distribution

Room temperature (RT) Mössbauer measurements, alone, are not adequate to differentiate Fe(III) in phyllosilicates in sediment from: (i) ferrihydrite and (ii) Al substituted goethite ($\chi_{Al} > 0.15$). Such differentiation cannot be made because all of these phases display doublet features at RT with similar Mössbauer parameters, rendering it difficult to discern their specific contributions. The presence and approximate amounts of these phases, however, can be resolved to varying degrees by comparing spectra obtained at lower temperatures, in combination with chemical data and other spectroscopic measurements. For example, ferrihydrite displays a doublet at 77 K (Murad and Cashion, 2004); illites display a doublet even at 4.2 K (e.g., Russell and Montano, 1978) whereas Al-substituted goethite ($\chi_{Al} > 0.15$; Fysh and Clark, 1982a; Kukkadapu et al., 2001) displays sextets at 77 K.

A comparison of the RT Mössbauer spectrum (Fig. 2a) of the pristine <2 mm FRC sediment with those obtained at lower temperatures (77, 12, and 5 K; Figs. 2b,c,d) indicated that the amount of "star-shaped" (large particle) goethite that was evident by microscopy in the clay-sized fraction of the sediment was not abundant overall (<1 wt%). Pure (e.g., without Al^{3+}substitution), large particle goethites display a sextet feature with a magnetic hyperfine field (B_{hf}) of 38.1 Tesla at RT (Murad and Cashion, 2004) that was absent in Fig. 2a. The lower temperature measurements revealed that the central doublet (0 to 1.2 mm/s region) of the RT spectrum had contributions from both phyllosilicate (illite, muscovite, and vermiculite) Fe(III), and Al-substituted goethite. Little or no Fe(III) was extracted from the sediment by AAO, which implied the absence of ferrihydrite.

The other RT Mössbauer doublet (0 to 2.6 mm/s region) with isomer shift (δ) = 1.3 mm/s and quadrupole shift (Δ) = 2.6 mm/s was due to silicate Fe(II) (Fig. 2a). The apparent Mössbauer parameters of the silicate Fe(III) and Fe(II) agreed well with illite/muscovite/vermiculite (Murad and Cashion, 2004). The vermiculite, muscovite, and illite peaks were not resolved from each other because they exhibit similar Mössbauer parameters (Greenwood and Gibb, 1971). The RT spectrum also indicated the presence of a small sextet (~5% of total area) from hematite. The derived quadrupole shift parameter (ε) and the B_{hf} values (−0.14 mm/s and 50.6 Tesla, respectively) of the small sextet were different from pure hematite (−0.2 mm/s and

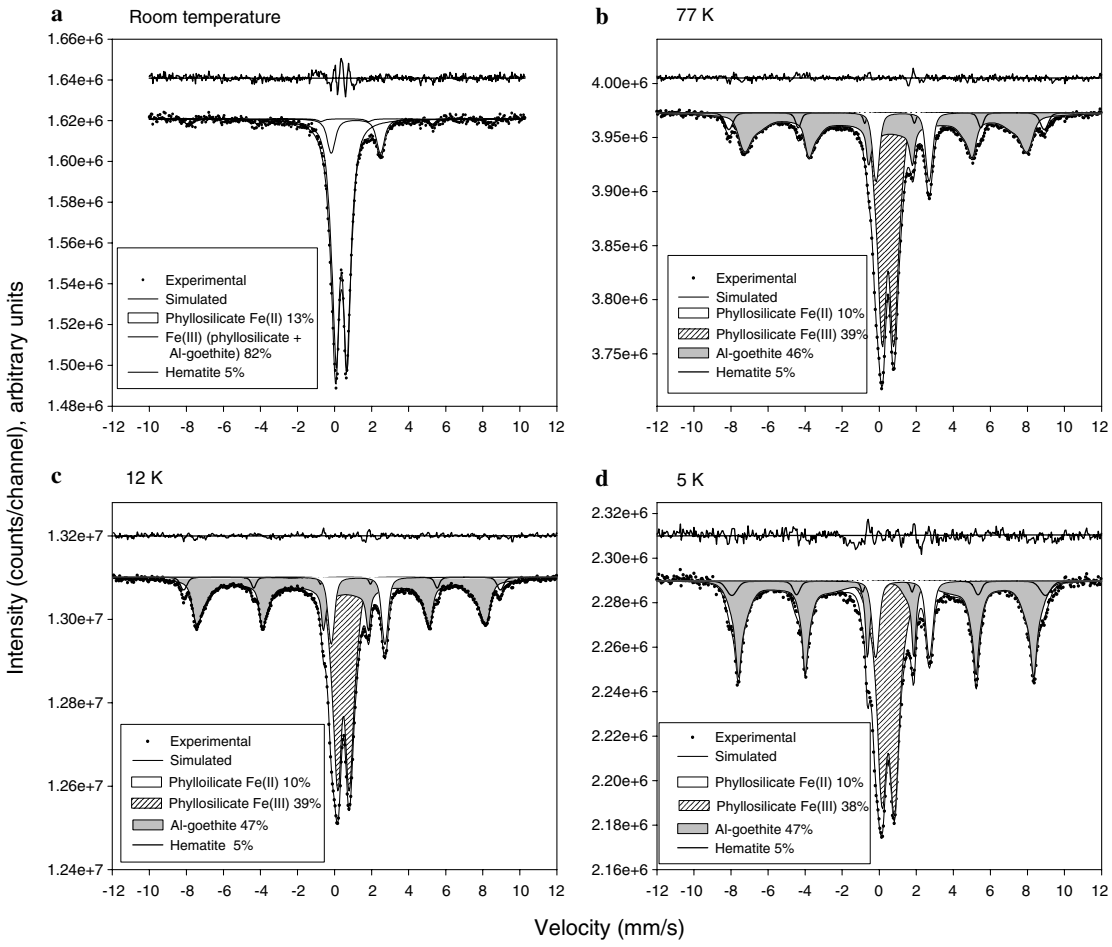

Fig. 2. Mössbauer spectra (experimental and simulated) of the <2.0 mm pristine sediment at RT, 77 K, 12 K, and 5 K.

51.8 Tesla; Murad and Cashion, 2004), possibly because of minor substitution of diamagnetic Al^{3+} for magnetic Fe^{3+} (Fysh and Clark, 1982b).

The low-temperature spectra were modeled to estimate the relative contents of goethite and phyllosilicate Fe, as well as the Fe(II)/Fe(III) ratio of the phyllosilicate. The spectra were modeled by the QSD/HFD method with one, two, and three Gaussian components, respectively, for phyllosilicate Fe(II), phyllosilicate Fe(III), and goethite sub-spectra, respectively, Table 1. The fit-derived Mössbauer parameters of phyllosilicate Fe and goethite (Table 2) agreed well with literature values. The spectral contributions, and accordingly the calculated mass percentages, of goethite (46–47% of Fe_{TOT}) and phyllosilicate Fe(II/III) (~50% of Fe_{TOT}) as well as the phyllosilicate Fe(II)/Fe(III) ratio (~0.25) were similar at all temperatures (77, 12, and 5 K; Fig. 2), given the assumption of equal Mössbauer recoilless fractions for all components. Other studies have reported variable effects of sample cooling on Mössbauer spectral areas of Fe-containing mineral components. Van der Zee et al. (2003) observed equivalent Mössbauer spectral areas of lake and marine sediments at RT and 4.2 K, while Wagner et al. (1988) noted that the Fe(III) oxide spectral area in Bavarian illite increased relative to phyllosilicate Fe(II) below 12 K. Differences in modeling approaches and assumptions may cause these apparent inconsistencies.

3.2. Effect of chemical reduction

Fe(III) oxides were extracted from the pristine sediment using DCB to verify the phase distributions derived from Mössbauer modeling and to provide additional Mössbauer information on Fe in the phyllosilicate fraction. DCB completely extracted goethite from the FRC sediment (Fig. 3). There was good agreement between the DCB-extracted Fe concentration (40% of Fe_{TOT}) and the Mössbauer spectral area of goethite (46% of Fe_{TOT} in Fig. 2). Hematite, however, was incompletely extracted from the sediment by DCB (Fig. 3). This recalcitrance may have been caused by its localization in inaccessible intraaggregate domains of the compact clasts. The Fe(II)/Fe(III) ratio of the phyllosilicate fraction was observed to increase from 0.25 in the pristine sediment to 0.5 after DCB treatment indicating that a fraction of the structural Fe(III) was susceptible to chemical reduction.

Table 1
Mössbauer fit parameters (δ_o, Δ, ε_o, σ_Δ, p_i, B_{hf}, σ_H, χ^2)[a]

Sample	Temp. (K)	Fe-species	δ_o (mm/s)	Δ or ε_o (mm/s)	σ_Δ (mm/s)	p_i (%)	B_{hf} (Tesla)	σ_H (Tesla)	χ^2 red.
Unreduced	77	Silicate Fe(II)	1.262	2.867	0.276	100	—	—	1.13
		Silicate Fe(III)	0.477	0.595	0.314	79.2	—	—	
				1.35	0.332	20.8	—	—	
		Goethite	0.485	−0.129	—	24.7	47.4	1.5	
						55.1	29.1	22.8	
						20	43.6	3.2	
		Hematite	0.478	−0.081	—	100	52.8	1	
	12	Silicate Fe(II)	1.272	2.894	0.249	100	—	—	1.57
		Silicate Fe(III)	0.482	0.557	0.28	56.8	—	—	
				1.05	0.48	43	—	—	
		Goethite	0.489	−0.125	—	23.2	48.4	1.1	
						53.6	33.4	24.9	
						23.2	45.8	2.5	
		Hematite	0.494	−0.092	—	100	53	0.8*	
	5	Silicate Fe(II)	1.262	2.90	0.286	100	—	—	1.96
		Silicate Fe(III)	0.49	0.641	0.37	69.7	—	—	
				1.42	0.8*	30.3	—	—	
		Goethite	0.495	−0.124	—	19.9	49.4	0.5	
						29.4	35.2	10	
						50.7	49.1	2.7	
		Hematite	0.424	0.036	—	100	52.5	1.5*	
Unreduced + DCB	5	Silicate Fe(II)	1.246	2.895	0.31*	88.5	—	—	1.32
				3.2*	0.5*	11.5	—	—	
		Silicate Fe(III)	0.49	0.693	0.468	100	—	—	
		Hematite	0.441	−0.016	—	100	52.1	2.05	
Bioreduced (60 d) (without AQDS)	12	Silicate Fe(II) + Fe(II) Biomineral	1.269	2.837	0.264	100	—		1.56
		Silicate Fe(III)	0.482	0.513	0.246	56.1	—	—	
				0.91	0.48	44	—	—	
		Goethite	0.492	−0.129	—	22	48.8	1	
						57.7	35.7	28.9	
						20	46.6	2.2	
		Hematite	0.486	−0.096	—	100	53.1	0.8*	
Bioreduced (60 d)** (without AQDS)	5	Silicate Fe(II)	1.263	2.893	0.141	100	—	—	1.24
		Goethite biotransformation product	1.182*	2.01*	—	100	7.87	3.59	
		Silicate Fe(III)	0.486	0.6	0.77	51.7	—	—	
				−0.68	0.14	48	—	—	
		Goethite	0.496	−0.126	—	57.7	49.32	0.87	
						42.3	35.7	18	
		Hematite	0.479	−0.054	—	100	53.34	0.0001*	
Bioreduced (95 d)** (with AQDS)	12	Silicate Fe(II)	1.289	2.926	0.08	62.7	—	—	1.77
		Fe(II) Biomineral		2.59	0.23	37			
		Silicate Fe(III)	0.503	0.593	0.27	100	—	—	
		Goethite	0.489	−0.164	—	52.4	48.4	1.34*	
						48	38.8	10.4*	
		Hematite	0.498	−0.103	—	100	52.9	0.8*	
Bioreduced (95 d)** (with AQDS)	5	Silicate Fe(II)	1.284	2.885	0	100	—	—	3.87
		Goethite biotransformation product	1.397	1.906	—	100	6.22	3.6*	
		Silicate Fe(III)	0.501	0.55	0.155	73.7	—	—	
				1.29	0.57	26.2	—	—	
		Goethite	0.489	−0.14	—	100	49.5	0.47	
		Hematite	0.471	−0.06	—	100	53.44	0	

[a] All parameters are as defined by Rancourt and Ping (1991). CS = $\delta_o + \delta_1(\Delta)$; Δ = center of QSD (quadrupole splitting distribution); $\varepsilon = \varepsilon_o + \varepsilon_1$ (B_{hf}); ε = center of quadrupole shift parameter; σ_Δ = sigma-width of QSD; B_{hf} = center of HFD (HFD = hyperfine field distribution); σ_H = sigma-width of HFD; halfwidth at half maximum (HWHM) = 0.097 mm/s; p_i = the percent of the ith Gaussian component of QSD/HFD; *this parameter was fixed during the fit; **HWHM = 0.2 mm/s.

Table 2
Fit-derived Mössbauer parameters ($\langle CS\rangle$, $\langle QS\rangle$, $\langle\varepsilon\rangle$, σ_{QSD}, $\langle B_{hf}\rangle$, and σ_{HFD})[a]

Sample	Temp. (K)	Fe-species	$\langle CS\rangle$[b] (mm/s)	$\langle QS\rangle$ or $\langle\varepsilon\rangle$ (mm/s)	σ_{QSD} (mm/s)	$\langle B_{hf}\rangle$ (Tesla)	σ_{HFD} (Tesla)
Unreduced	77	Silicate Fe(II)	1.262	2.867	0.276	—	—
		Silicate Fe(III)	0.477	0.757	0.431	—	—
		Goethite	0.485	−0.129	—	37.75	16.39
		Hematite	0.478	−0.081	—	52.78	1.03
	12	Silicate Fe(II)	1.272	2.894	0.249	—	—
		Silicate Fe(III)	0.482	0.777	0.445	—	—
		Goethite	0.489	−0.125	—	40.9	17.11
		Hematite	0.494	−0.092	—	53.02	0.8
	5	Silicate Fe(II)	1.262	2.903	0.286	—	—
		Silicate Fe(III)	0.49	0.893	0.623	—	—
		Goethite	0.496	−0.124	—	45.09	8.57
		Hematite	0.424	0.036	—	52.49	1.5
Unreduced + DCB	5	Silicate Fe(II)	1.246	2.93	0.353	—	—
		Silicate Fe(III)	0.49	0.721	0.422		
		Hematite	0.441	−0.016	—	52.08	2.05
Bioreduced (60 d) (without AQDS)	12	Silicate Fe(II) + Fe(II) Biomineral	1.27	2.837	0.264	—	—
		Silicate Fe(III)	0.482	0.694	0.407	—	—
		Goethite	0.492	−0.129	—	42.52	19.35
		Hematite	0.486	−0.096	—	53.13	0.8
Bioreduced (60 d) (without AQDS)	5	Silicate Fe(II)	1.263	2.892	0.149	—	—
		Goethite Biotransformation product	1.182	2.01	—	7.9	3.51
		Silicate Fe(III)	0.486	0.715	0.448	—	—
		Goethite	0.496	−0.126	—	41.33	14.36
		Hematite	0.479	−0.054	—	53.34	1E − 04
Bioreduced (95 d) (with AQDS)	12	Silicate Fe(II) + Fe(II) Biomineral	1.289	2.85	0.229	—	—
		Silicate Fe(III)	0.503	0.596	0.426	—	—
		Goethite	0.489	−0.164	—	43.79	8.69
		Hematite	0.498	−0.103	—	52.87	0.8
Bioreduced (95 d) (with AQDS)	5	Silicate Fe(II)	1.284	2.884	0.003	—	—
		Goethite Biotransformation product	1.397	1.906	—	6.34	3.37
		Silicate Fe(III)	0.501	0.745	0.455	—	—
		Goethite	0.489	−0.14	—	49.45	0.47
		Hematite	0.471	−0.061	—	53.44	0.042

[a] $\langle CS\rangle$ = average center shift; $\langle QS\rangle$ = average quadrupole shift; $\langle\varepsilon\rangle$ = average quadrupole shift parameter; σ_{QSD} = standard deviation of QS; $\langle B_{hf}\rangle$ = average hyperfine field; and σ_{HFD} = standard deviation of hyperfine field distribution.
[b] With respect to metallic 20-μm Fe foil at RT.

3.3. Sediment bioreduction

3.3.1. Incubation in bicarbonate buffer

The FRC background sediment was incubated with *S. putrefaciens* under anoxic conditions in the absence and presence of AQDS which is known to stimulate the rate and extent of Fe(III) bioreduction in natural sediments (Zachara et al., 1998; Kukkadapu et al., 2001). Ten to fifteen percent of $Fe(III)_{TOT}$ (based on 0.5 N HCl extraction) was reduced in 60 d without AQDS, whereas 24% and 35% of $Fe(III)_{TOT}$ was bioreduced after 40 and 95 d incubations in media that contained AQDS. The concentrations of aqueous Fe^{2+}, Mn(II), Si, Al, and Mg, were at or near detection limits for all treatments during the entire incubation period.

Powder XRD patterns of the bioreduced sediments (not shown) were almost identical to the pristine material, despite significant reduction. The unreduced and bioreduced samples, however, differed from each other in their Mössbauer spectra (Fig. 4). The doublet feature caused by Fe(II) (denoted by *) was more intense in the bioreduced samples at RT and 12 K. The sediment incubated with AQDS displayed an even greater enhancement in the Fe(II) signal [compare Fe(II) spectral area of Fig. 5b with Fig. 5a; 46% vs. 21%]. The increase in the Fe(II) doublet in the 12 K spectra (Fig. 5) was accompanied by a reduction in the spectral area of both the goethite sextet and phyllosilicate Fe(III) [compare fit-derived spectral areas of the bioreduced samples (Figs. 5a and b) to the pristine sediment (Fig. 2c)]. The increase in the spectral area of Fe(II)

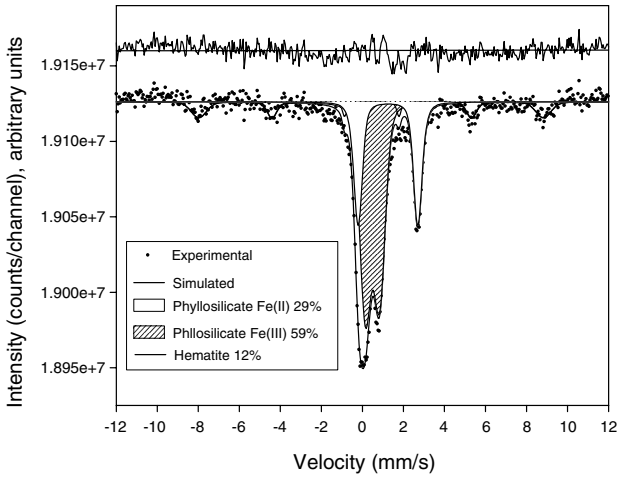

Fig. 3. Experimental and simulated 5 K Mössbauer spectra of the <2.0 mm pristine sediment treated with DCB.

represented the biotransformation products of both of goethite and phyllosilicate Fe(III), with each exhibiting similar Mössbauer parameters at RT. A reasonably good fit of the Fe(II) doublet was obtained with a two Gaussian component HFD distribution, implying the presence of two components.

The relative contributions of phyllosilicate Fe(II) and the biotransformation product were resolved from each other at liquid helium temperature (5 K) where a magnetically ordered phase was observed (Figs. 5c,d). The spectral area of the biogenic Fe(II) product was fourfold higher in the sediment incubated with AQDS (24% vs. 6% of Fe_{TOT} without AQDS). There was qualitative agreement between the mass loss of goethite (30%) and the amount of biogenic Fe(II) product formation (24%) as deduced by spectral modeling implying that goethite was the source of the biotransformation product. Perhaps the *f*-factors of phyllosilicate Fe(II) and the biogenic Fe(II) phases were different. The spectral area of hematite was unchanged in incubations with and without AQDS.

The phyllosilicate Fe(II) concentration (17–20%) was comparable in the samples incubated with and without AQDS, and both of these were higher than the pristine sediment (10%). Accordingly, the computed phyllosilicate Fe(II)/Fe(III) ratio in bioreduced sediments was higher than the pristine sediment (~0.6 vs. 0.25). This increase in the phyllosilicate Fe(II)/Fe(III) ratio corresponded to the reduction of ~20% of the total structural phyllosilicate Fe(III) to Fe(II). The Fe(II)/Fe(III) ratio was similar for sediments incubated without AQDS (0.58) and with AQDS

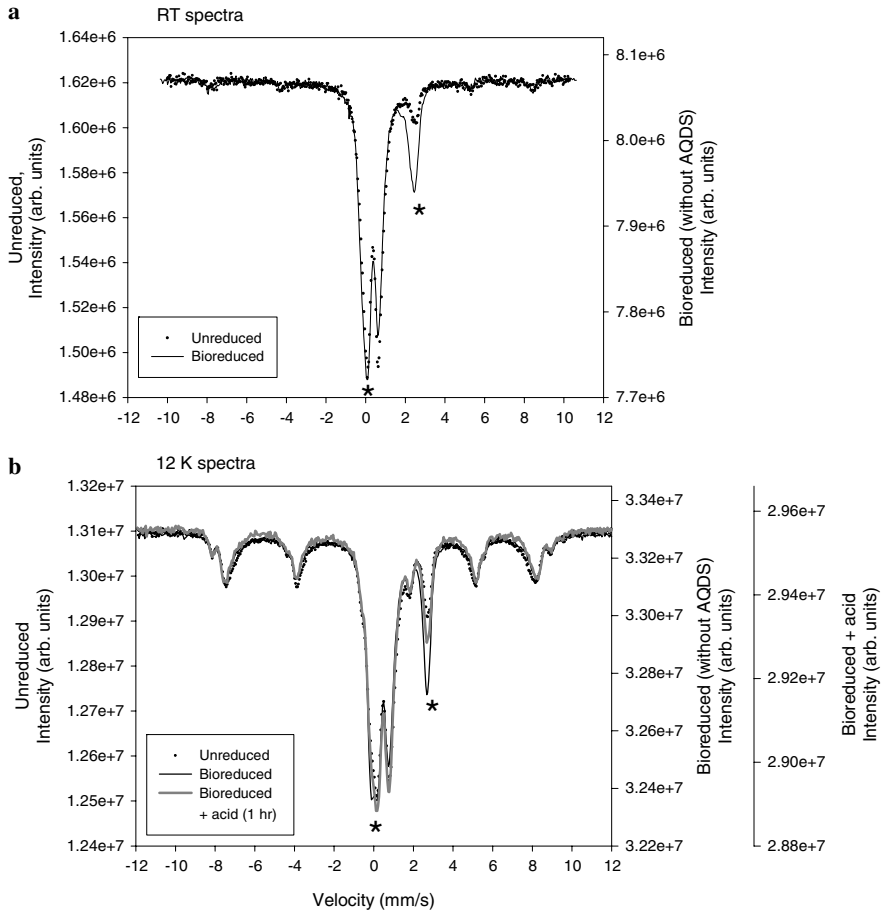

Fig. 4. Mössbauer spectra of pristine, bioreduced (without AQDS) and acid-treated, bioreduced sediment: (a) Room temperature, and (b) 12 K.

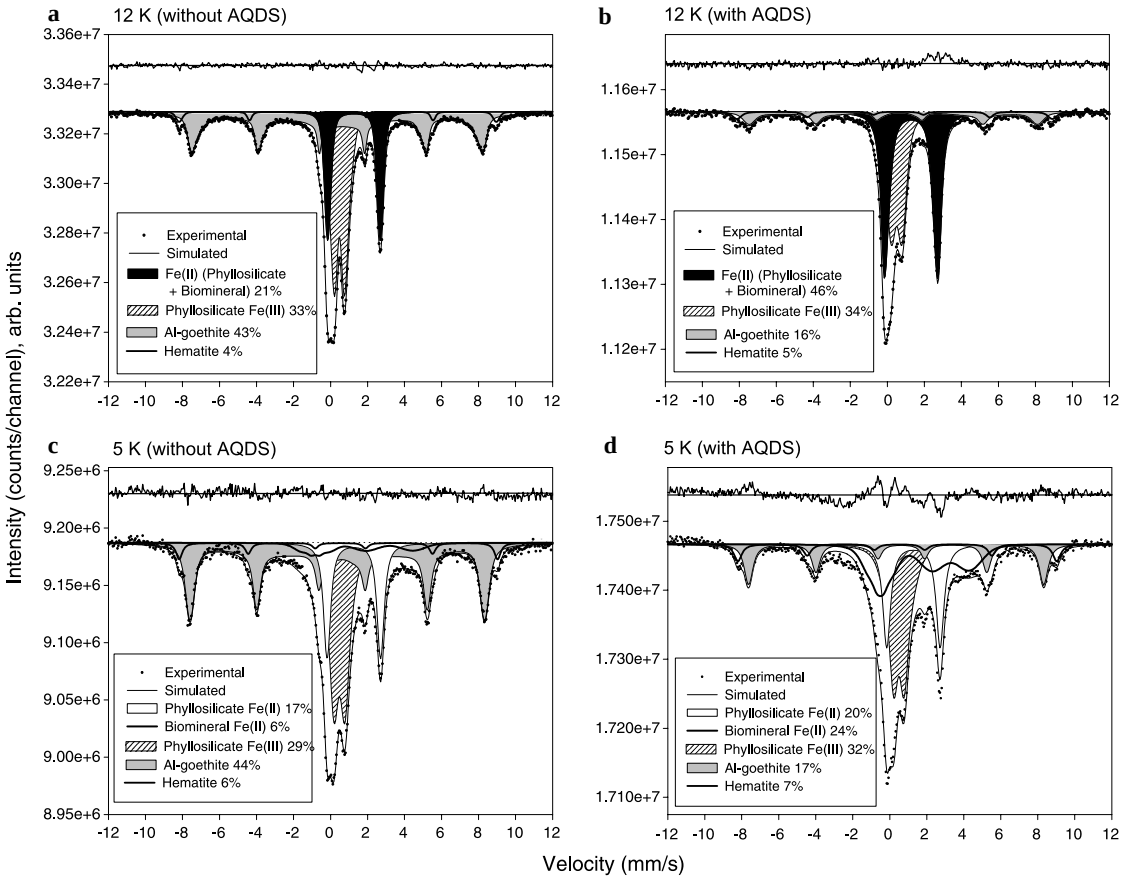

Fig. 5. Mössbauer spectra (experimental and simulated) of bioreduced sediments with and without AQDS: (a) 12 K spectrum of the 60-d sample without AQDS; (b) 12 K spectrum of the 95-d sample with AQDS; (c) 5 K spectrum of the 60-day sample without AQDS, and (d) 5 K spectrum of the 95-d sample with AQDS.

(0.62), and these, in turn, were comparable to the DCB-treated sediment (~0.5; Fig. 3).

3.3.2. Incubation in PIPES buffer

The pristine sediment was also incubated with CN32 in PIPES buffer without AQDS to determine if the buffer assisted formation or caused discernable differences in the nature of the sorbed biogenic Fe(II) pool. The course of bioreduction was identical in PIPES buffer as compared to the bicarbonate buffer in that Fe(III) reduction began when Mn(III/IV) was exhausted. The rate and extent of Fe(III) bioreduction, however, differed in the two buffers. Less than 10% of Fe_{TOT} was reduced by CN32 after 60 d of incubation in the PIPES-buffered medium as compared to ~15% in the bicarbonate-buffered medium, as determined by 0.5 N HCl extraction. This difference was evident in the Mössbauer spectral intensities of the Fe(III) and Fe(II) doublets of the 60-d bioreduced sediments from PIPES- and bicarbonate-buffered suspensions (not shown).

Calcium chloride extraction was performed on the bioreduced sediment from PIPES-buffer to determine whether ion exchangeable Fe(II) was present. Very small amounts of Fe(II) [<1% of the 0.5 N HCl extractable Fe(II)] were extracted, indicating that most biogenic Fe(II) did not exist in an ion-exchangeable state. Calcium chloride extraction was not carried out with the sediment incubated in the bicarbonate buffer because of concern for ferroan–$CaCO_3$ precipitation.

3.3.3. Acid treatment of the chemically and biologically reduced sediments

Weak acid (0.5 N HCl) is used to extract "bioavailable Fe(III) oxide" from oxidized sediments (Anderson et al., 1998; Anderson and Lovley, 1999), and various Fe(II) forms from reduced sediments/clays/Fe-oxides including: adsorbed and precipitated Fe(II) phases (e.g., Fredrickson et al., 1998; Zachara et al., 1998; Komlos and Jaffe, 2004; Kukkadapu et al., 2004; Jaisi et al., 2005; Seabaugh et al., 2006). Acid extraction (0.5 N HCl for 1 h) was performed on the unreduced sediment to estimate the "bioavailable Fe(III) oxide" content (ferrihydrite primarily) and to determine phyllosilicate phase stability in weak acid. It was also performed on the bioreduced sediments to quantify biogenic Fe(II) and to follow possible bioreduction-induced changes in the acid-stability of the phyllosilicate structure.

Little or no Fe, Si, Al or Mg was extracted from pristine sediment by the weak acid, confirming that both goethite

and the phyllosilicate phases were stable towards 0.5 N HCl, and documenting the absence of ferrihydrite. However, acid extraction removed significant amounts of Si, Al, and Mg along with the Fe(II) from the bioreduced sediments (Table 3). Little or no Fe(III) was observed in any of the 1 h-weak acid extractions of the bioreduced sediment. The extracted cations were presumed to result from the dissolution of fine-grained phyllosilicates whose structure was rendered "more soluble" by complete structural Fe(III) reduction. AQDS had little or no effect on the acid-extractable concentrations of Si, Al, Mn and Mg, but markedly enhanced acid-extractable Fe(II). It was therefore implied that AQDS enhanced goethite bioreduction without impacting phyllosilicate reduction. This finding contrasts with that of Dong et al. (2003) who observed enhanced bioreduction of illite by CN32 when AQDS was present.

Mössbauer analysis of the acid-treated, bioreduced sediment (60 d without AQDS; Fig. 4b) displayed marked reductions in the Fe(II) doublet relative to the unextracted, bioreduced sample. The computed Fe(II)/Fe(III) ratio of the acid-treated, bioreduced sediment was 0.33 as compared to 0.25 for the pristine sediment and ~0.6 for the bioreduced sediments. These observations implied that: (i) the observed phyllosilicate Fe(II)/Fe(III) ratio of bioreduced samples (~0.6) represented an average state containing unreduced [Fe(II)/Fe(III) = 0.25] and completely reduced phyllosilicate domains [$Fe(II)/Fe_{TOT} \sim 1$], and (ii) weak acid dissolved only those phyllosilicates, or domains within them, where structural Fe(III) was fully reduced. The slightly higher phyllosilicate Fe(II)/Fe(III) ratio of the acid-treated, bioreduced sediment (0.33) as compared to the pristine sediment (0.24) was probably due to incomplete dissolution of reduced phyllosilicate domains in the 1 h extraction (Komlos and Jaffe, 2004).

The acid induced (0.5 N HCl) dissolution behavior of the DCB-treated pristine sediment (Fig. 6) lent support to our conceptual model of reduced and unreduced phyllosilicate domains in the bioreduced sediment. The strong DCB reductant extracted most of the Fe(III) oxides, and reduced a portion of the structural Fe(III) to structural Fe(II) in the phyllosilicates (Fig. 3). On acid contact, the DCB-treated sediment rapidly released Fe(II), Al, and Si that were presumed to originate in an accessible, high-surface area phyllosilicate phase that was reactive with dithionite. The absence of Fe(III) at time periods of less than 24 h indicated that Fe in this acid-soluble phyllosilicate was fully reduced. The dissolution rate slowed after 24 h and increasing concentrations of Fe(III) were observed in the extracts, while Fe(II) concentrations remained constant. This later stage was consistent with the dissolution of larger particle-sized illites and micas whose Fe(II)/Fe(III) ratios were less or uneffected by DCB treatment.

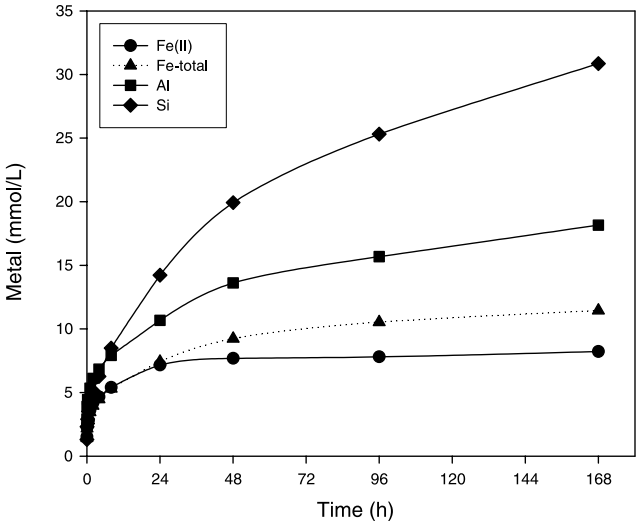

Fig. 6. Acid extractable solutes (Fe^{2+}, Fe_{TOT}, Si, and Al) from the DCB-treated pristine sediment.

4. Discussion

4.1. Mineral electron acceptors for bacterial Fe(III) respiration

The studied sediment contained a mixture of millimeter-sized aggregates of contrasting mineralogy and physical properties, and different total iron contents. The relative percentages of the two clast types were not quantitatively determined, but they appeared to be present in nominally equal abundances. Weathered clasts were present with large open internal pores, large mineral crystallites (e.g., >10 μm), and Fe-containing micas. These clasts would appear to offer a physical environment conducive to intraparticle bacterial colonization, but their average total Fe content was three times less (2.12 wt%) than the other predominant clast type (6.12 wt%). The compact clasts contained a fine-textured groundmass of Fe-containing illite with imbedded crystallites of nano-meter sized Fe(III) oxides. With negligible internal porosity, these clasts offered a significant challenge of accessibility to organisms that require direct contact for reduction. We have previously observed (Fredrickson et al., 2004) that Tc(VII) reduction by "sorbed" Fe(II) in the bioreduced FRC sediment occurs

Table 3
Concentration of acid soluble Fe, Mn, Si, Al and Mg

Bioreduced sediment	Fe (mM)	Mn (mM)	Si (mM)	Mg (mM)	Al (mM)
60 d (without AQDS)	12.1	4.8	4.9	4	12
40 d (with AQDS)	20.1	4.9	4.8	4.6	12.2
95 d (with AQDS)	28.5	5.9	5.4	5.3	14.1

preferentially within the weathered clasts, possibly indicating that bacterial Fe(III) reduction was higher in those domains.

On a bulk basis, approximately 50% of the Fe_{TOT} was present as goethite, with the remainder residing in phyllosilicates. A disproportionate fraction of the Fe(III) resided in the compact clasts. EMP analyses indicated that phyllosilicate Fe existed in illite and mica, at minimum. Iron may also exist in the vermiculites and HIV evident by XRD, but these phases were difficult to unequivocally identify by electron microscopy and compositional analysis was not performed. Given the diagenetic relationship between micas, vermiculites, and HIV in acid soils (Barnhisel and Bertsch, 1989), it is probable that the observed vermiculites and HIV were iron substituted as well. The clast locations of the vermiculite components were not determined. A small amount of hematite (<5% of Fe_{TOT}) was also present, and its partial recalcitrance to DCB extraction indicated that, like goethite, it resided in the compact clasts.

The partial reduction of both goethite and phyllosilicate Fe(III) by CN32 was evident from the 5 K Mössbauer spectra (Figs. 5c,d). We were unable to determine which specific phyllosilicate phase was bioavailable, but the observance of considerable weak-acid extractable Si, Al, and Mg (Table 3) indicated that structural Fe(III) in a fraction of the phyllosilicates was completely reduced. Complete Fe reduction caused the phyllosilicates to be more soluble in weak acid. Goethite and phyllosilicate Fe(III) were reduced to equal extents in the 60 d incubation that was not amended with AQDS where approximately 10–15% of the $Fe(III)_{TOT}$ was reduced (Figs. 5a,c). Hence, there was no apparent bacterial preference for a specific mineralogic electron acceptor based on accessibility or free energy.

4.2. Aggregation effects on Fe(III)-mineral bioavailability

AQDS readily enters the electron transport chain of DMRB (DiChristina et al., 2005), including *Shewanella* and is rapidly reduced to AH_2DS. AH_2DS is a soluble reductant that can access electron acceptors in pore and intragrain space that is below the nominal size of CN32 (e.g., 0.3×2.0 μm) by either advection or diffusion. The extent of mineral Fe(III) bioreduction in the FRC sediment was threefold greater in media that contained AQDS. AQDS enhanced the bioreduction of goethite, but had no appreciable effect on phyllosilicate reduction. Goethite was found primarily in the compact clasts of the FRC sediment. Direct bacterial contact with goethite that was in the interiors of such aggregates with small internal porosity was limited in the incubations with CN32 alone. This access limitation was relieved by AQDS. AQDS enhanced the bioreduction of goethite and hematite in sand-textured subsurface sediments from the Atlantic coastal plain (Zachara et al., 1998) by a comparable mechanism. Why hematite in the FRC sediment was not reduced by AH_2DS is unclear.

The observed commonality in the phyllosilicate Fe(II)/Fe(III) ratio (0.57 ± 0.06) of the three reduced sediments (CN32, CN32/AQDS, and DCB) was unexpected. Prior to experiment we speculated that reduction extent would be greatest in the DCB and AQDS treatments because of the ability of soluble reductants to access intraparticle, fine-grained phyllosilicates in the compact clasts, as noted above for goethite. Supporting this hypothesis was the work of Dong et al. (2003) who found that AQDS enhanced the bioreduction of both illite and goethite by CN32 in a mixture of these phases. Although we do not know the specific phyllosilicate phase that was reduced in the FRC sediment (e.g., vermiculite, HIV, or illite), it appears that: (i) the same phase or phase mixture was redox active towards both CN32 or dithionite, and (ii) the total amount of phyllosilicate Fe(III) that was reducible was controlled by mineral physical and/or chemical factors [e.g., it was limited to a maximum Fe(II)/Fe(III) ratio of 0.6].

Accessibility appeared as a minor factor influencing phyllosilicate bioreduction, in spite of the presence of copious fine-grained phyllosilicates in internal domains of the compact clasts. *S. putrefaciens* is known to produce soluble reductants under certain conditions (e.g., Newman and Kolter, 2000; Nevin and Lovley, 2000) and perhaps these were produced here allowing intra-aggregate access to phyllosilicates (and goethite) in the CN32 incubations without AQDS. To be consistent with the observed results, however, the soluble reductants would have had to exhibit a higher effective redox potential, or been present in significantly lower concentration than AQDS.

4.3. The biotransformation product of goethite

The lack of extractability of sorbed biogenic Fe(II) by $CaCl_2{\cdot}2H_2O$ suggested that it was a strongly sorbed or precipitated phase and not an ion exchange complex. Mössbauer measurements also supported this conclusion. Ion exchangeable Fe(II) in smectite suspensions is "invisible" to Mössbauer spectroscopy at RT because of a low recoil fraction (Diamant et al., 1982). Accordingly, the presence of an ion-exchangeable Fe(II) component on bioreduced nontronite was deduced from a noted increase in the spectral intensity of Fe(II) as measurement temperature was lowered (Jaisi et al., 2005). In contrast, we observed similar spectral areas for Fe(II) in bioreduced sediments at RT and 12 K which was not consistent with ion exchangeable Fe(II) as a principal component.

The Mössbauer doublets of phyllosilicate Fe(II) and the biogenic Fe(II) phase were not well-resolved from each other at >12 K, making it difficult to identify the biogenic Fe(II) material from the higher temperature spectra. The presence of a distinct adsorbed or precipitated biogenic Fe(II) phase, however, was evident at 5 K from magnetic ordering that broadened the spectra from −5 to +6 mm/s (Fig. 5), and lowered the contribution of the Fe(II) doublet feature to the overall spectra. Comparable magnetic

ordering was not observed in the DCB-treated sample at 5 K (Fig. 3), ruling out phyllosilicate Fe(II) as the source of this spectral feature. The extent of magnetic ordering was proportional to the decrease in the spectral area of goethite, suggesting that the transformation of goethite by CN32 or bioreduced AQDS was the source of this product. Moreover, commonality in the Mössbauer parameters of the various peaks observed in the 5 K spectra of the bioreduced sediments without and with AQDS, indicated that the nature of this phase was the same in both materials, and therefore, not solely a consequence of biomineralization induced by direct cellular contact.

The identity of the biogenic Fe(II) mineral product could not be definitively determined by Mössbauer measurements at 5 K. The biogenic Fe (II) product was not any of the previously identified biomineralization products of Fe(III) oxides. It was not siderite ($FeCO_3$), a biomineralization product that might be expected to precipitate in the bicarbonate buffer used here, and as noted recently by Peretyazhko and Sposito (2005) in soils that underwent Fe(III) reduction. Siderite displays a distinct Mössbauer sextet at 12 K and higher δ and Δ, and lower B_{hf} values than goethite (Wade et al., 1999). The absence of Fe(III) in the weak acid extract indicated that the transformation product was also not green-rust (GR), a mixed Fe(II)/Fe(III) phase, even though the fit-derived Mössbauer parameters at 77 K matched well with GR-like compounds (e.g., Ona-Nguema et al., 2002; Kukkadapu et al., 2004). The Mössbauer parameters of the biogenic Fe(II) phase were also not consistent with fayalite [$Fe(II)_2SiO_4$; e.g., Ericsson and Khangi, 1988] that magnetically orders at 77 K, or greenalite [$Fe(II)_{2.3}Fe(III)_{0.5}Si_{2.2}O_5(OH)_{3.3}$] (e.g., Ballet and Coey, 1978). The Mössbauer parameters and solubility behavior of the biogenic Fe phase also did not agree with $Fe(OH)_2$ (Koch, 1998). The presence of magnetite was further ruled out because little Fe(III) was extracted by 0.5 N HCl acid. The observed magnetic ordering at 5 K was inconsistent with spectra of Fe(II) adsorbed on bacterial cell surfaces (Rancourt et al., 2005) that displays a doublet at liquid He temperature. Additionally, the amount of biogenic Fe(II) was in large excess compared to the sorption capacity of the cells (Liu et al., 2001).

It is possible that the biogenic Fe(II) phase remained in association with goethite in the sediment, its apparent mineralogic source, because soluble Fe(II) was not observed during the entire course of reductive incubation. The temperature response and Mössbauer spectral signature of the biogenic Fe(II) phase resembled that of an "adsorbed Fe(II)" phase observed by Williams et al. (2005) in bioreduced ferrihydrite containing siderite and magnetite. This unidentified phase displayed comparable Mössbauer parameters at 4.2 K to our biogenic Fe(II) phase at 5 K. While Fe(II) adsorbed on an Fe(III) oxide surface would magnetically order at liquid He temperature due to spin polarization with the substrate (Rancourt et al., 2005); we feel that the concentration of the biogenic Fe(II) phase in our studied sediment was well above that which can be rationalized as an adsorbed phase (e.g., a surface complex) on the residual goethite. Considerations of surface site concentration mandate that the phase be a precipitate, possibly associated directly with the goethite surface. We speculate that the phase could be a Fe(II)-rich, Fe(II)–Al coprecipitate, with Al originating from the aluminous goethite. This phase would be different from that observed by Williams et al. (2005), as their experimental system did not contain Al. Efforts continue in our laboratory to identify this phase, as it may be of significant general importance.

5. Conclusions

The dissimilatory metal reducing bacteria, *S. putrefaciens* strain CN32, was able to access various Fe(III) forms in a physically aggregated, mineralogically complex shale–limestone saprolite. Both goethite and Fe(III) containing phyllosilicates were utilized as electron acceptors for lactate oxidation. In the absence of an electron shuttle, approximately 50% of the bioreduction was associated with phyllosilicate Fe(III) and the remainder with goethite. These mineral phases exhibited complex physical distribution at the surfaces of and within aggregates of fine-grained crystallites and their potential interfacial surface areas could not be readily estimated. Consequently it was not possible to evaluate whether there was competition between these phases for electron equivalents, or the primary factors controlling bacterial utilization of different mineral Fe(III) forms. Experimental evidence strongly suggested that *Shewanella* was able to access intra-aggregate Fe(III), either through colonization of larger pores or release of a soluble reductant.

Reductive biologic activity yielded two primary mineral products: (i) fine-grained phyllosilicate domains where all structural Fe was reduced and that were soluble in 0.5 N HCl, and (ii) a biotransformation product of goethite exhibiting magnetic ordering in its 5 K Mössbauer spectrum. The goethite-derived phase was not identified because it exhibited different characteristics from all known Fe(III) oxide transformation products. The lack of extractability of sorbed Fe(II) in $CaCl_2{\cdot}2H_2O$ and its Mössbauer response at various temperatures indicated that goethite biotransformation product was not an adsorbed Fe(II) species on the surfaces of phyllosilicates. Additional characterization [e.g., application of applied-field Mössbauer spectroscopy where better resolution of phyllosilicate and biogenic Fe(II) peaks is expected], and experiments (e.g., biotransformation studies of Al-substituted goethite and low temperature Mössbauer measurements) are needed for more definitive identification of this curious biogenic Fe(II) product. Either one or both of these biotransformation products are responsible for the rapid heterogeneous reduction of Tc(VII) noted in sediments treated similarly in the lab (Fredrickson et al., 2004). These phases are also the most likely mineral products formed through in situ stimulation of the endogenous Fe(III)-reducing bacteria

in the field site from which these sediments were obtained (Istok et al., 2004).

Acknowledgments

This research was supported by the Natural and Accelerated Bioremediation Research Program (NABIR), Office of Biological and Environmental Research (OBER), US Department of Energy (DOE). Mössbauer and XRD measurements were performed at the W.R. Wiley Environmental Molecular Sciences Laboratory (EMSL), a DOE national scientific user facility. PNNL is operated for the Department of Energy by Battelle. We thank Associate Editor, Jeremy Fein and anonymous reviewers for their help in improving the manuscript.

Associate editor: Jeremy B. Fein

References

Amonette, J.E., Workman, D.J., Kennedy, D.W., Fruchter, J.S., Gorby, Y.A., 2000. Dechlorination of carbon tetrachloride by Fe(II) associated with goethite. *Environ. Sci. Technol.* **34**, 4606–4613.

Anderson, R.T., Rooney-Varga, J.N., Gaw, C.V., Lovley, D.R., 1998. Anaerobic benzene oxidation in the Fe(III) reduction zone of petroleum-contaminated aquifers. *Environ. Sci. Technol.* **32**, 1222–1229.

Anderson, R.T., Lovley, D.R., 1999. Naphthalene and benzene degradation under Fe(III)-reducing conditions in petroleum-contaminated aquifers. *Bioremediation J.* **3**, 121–135.

Ballet, O., Coey, J.M.D., 1978. Greenalite—a clay showing two-dimensional magnetic order. *J. Phys. Colloq.* **39** (C6), 765–766.

Barnhisel, R.I., Bertsch, P.M., 1989. Chlorites and hydroxy-interlayered vermiculite and smectites. In: Dixon, J.B., Weed, S.B. (Eds.), *Minerals in Soil Environments*. SSSA, Madison, WI, pp. 729–788.

Cervini-Silva, J., Larson, R.A., Wu, J., Stucki, J.W., 2001. Transformation of chlorinated aliphatic compounds by ferruginous smectite. *Environ. Sci. Technol.* **35**, 805–809.

Cooper, C.D., Neal, A.L., Kukkadapu, R.K., Brewe, D., Coby, A., Picardal, F.W., 2005. Effects of sediment iron mineral composition on microbially mediated changes in divalent metal speciation: importance of ferrihydrite. *Geochim. Cosmochim. Acta* **69**, 1739–1754.

Diamant, A., Pasternak, M., Banin, A., 1982. Characterization of adsorbed iron in montmorillonite by Mössbauer spectroscopy. *Clays Clay Miner.* **30**, 63–66.

DiChristina, T.J., Fredrickson, J.K., Zachara, J.M., 2005. Enzymology of electron transport: energy generation with geochemical consequences. *Rev. Mineral. Geochem.* **59**, 27–52.

Dong, H., Kukkadapu, R.K., Fredrickson, J.K., Zachara, J.M., Kennedy, D.W., Kostandarithes, H., 2003. Microbial reduction of structural Fe(III) in illite and goethite. *Environ. Sci. Technol.* **37**, 1266–1276.

Ericsson, T., Khangi, F., 1988. An investigation of $Fe_3(PO_4)_2$–Sarcopside between 1.6 K–721 K: comparison with fayalite. *Hyperfine Interact.* **41**, 783–786.

Favre, F., Tessier, D., Abdelmoula, M., Genin, J.M., Gates, W.P., Boivin, P., 2002. Iron reduction and changes in cation exchange capacity in intermittently waterlogged soil. *Eur. J. Soil Sci.* **58**, 175–183.

Fredrickson, J.K., Zachara, J.M., Kennedy, D.W., Dong, H., Onstott, T.C., Hinman, N.W., Li, S.W., 1998. Biogenic iron mineralization accompanying the dissimilatory reduction of hydrous ferric oxide by a ground water bacterium. *Geochim. Cosmochim. Acta* **62**, 3239–3257.

Fredrickson, J.K., Zachara, J.M., Kennedy, D.W., Duff, M.C., Gorby, Y.A., Li, S.W., Krupka, K.M., 2000. Reduction of U(VI) in goethite (α-FeOOH) suspensions by a dissimilatory metal-reducing bacterium. *Geochim. Cosmochim. Acta* **64**, 3085–3098.

Fredrickson, J.K., Zachara, J.M., Kukkadapu, R.K., Gorby, Y.A., Smith, S.C., Brown, C.F., 2001. Biotransformation of Ni-substituted hydrous ferric oxide by an Fe(III)-reducing bacterium. *Environ. Sci. Technol.* **35**, 703–712.

Fredrickson, J.K., Zachara, J.M., Kennedy, D.W., Kukkadapu, R.K., McKinley, J.P., Heald, S.M., Liu, C., Plymale, A.E., Smith, S.C., 2004. Reduction of TcO_4^- by sediment-associated biogenic Fe(II). *Geochim. Cosmochim. Acta* **68**, 3171–3187.

Fysh, S.A., Clark, P.E., 1982a. Aluminous goethite: a Mössbauer study. *Phys. Chem. Miner.* **8**, 180–187.

Fysh, S.A., Clark, P.E., 1982b. Aluminous hematite: a Mössbauer study. *Phys. Chem. Miner.* **8**, 257–267.

Greenwood, N.N., Gibb, T.C., 1971. *Mössbauer Spectroscopy*. Chapman and Hall, London.

Haderlein, S.B., Pecher, K., 1998. Pollutant reduction in heterogeneous Fe(II)–Fe(III) systems. In: Sparks, D.L., Grundl, T.J. (Eds.), *Mineral–Water Interfacial Reactions: Kinetics and Mechanisms*. American Chemical Society, pp. 342–356.

Hofstetter, T.B., Neumann, A., Schwarzenbach, R.P., 2006. Reduction of nitroaromatic compounds by Fe(II) species associated with iron-rich smectites. *Environ. Sci. Technol.* **40**, 235–242.

Istok, J.D., Senko, J.M., Krumholz, L.R., Watson, D., Bogle, M.A., Peacock, A., Chang, Y.J., White, D.C., 2004. In situ bioreduction of technetium and uranium in a nitrate-contaminated aquifer. *Environ. Sci. Technol.* **380**, 468–475.

Jaisi, D.P., Kukkadapu, R.K., Eberl, D.E., Dong, H., 2005. Control of Fe(III) site occupancy on the rate and extent of microbial reduction of Fe(III) in nontronite. *Geochim. Cosmochim. Acta* **69**, 5429–5440.

Jeon, B.H., Kelly, S.D., Kemner, K.M., Barnet, M.O., Burgos, W.D., Dempsey, B.A., Roden, E.E., 2004. Microbial reduction of U(VI) at the solid–water interface. *Environ. Sci. Technol.* **38**, 5649–5655.

Koch, C.B., 1998. Structure and properties of anionic clays. *Hyperfine Interact.* **117**, 131–158.

Komlos, J., Jaffe, P.R., 2004. Effect of iron bioavailability on dissolved hydrogen concentrations during microbial iron reduction. *Biodegradation* **15**, 315–325.

Kostka, J.E., Stucki, J.W., Nealson, K.H., Wu, J., 1996. Reduction of structural Fe(III) in smectite by a pure culture of *Shewanella putrefaciens* strain MR-1. *Clays Clay Miner.* **44**, 522–529.

Kostka, J.E., Haefele, E., Viehweger, R., Stucki, J.W., 1999. Respiration and dissolution of iron(III) containing clay minerals by bacteria. *Environ. Sci. Technol.* **33**, 3127–3133.

Kukkadapu, R.K., Zachara, J.M., Smith, S.C., Fredrickson, J.K., Liu, C., 2001. Dissimilatory bacterial reduction of Al-substituted goethite in subsurface sediments. *Geochim. Cosmochim. Acta* **65**, 2913–2924.

Kukkadapu, R.K., Zachara, J.M., Fredrickson, J.K., Kennedy, D.W., 2004. Biotransformation of synthetic 2-line silica–ferrihydrite coprecipitates by a dissimilatory Fe(III)-reducing bacterium: formation of carbonate green rust in the presence of phosphate. *Geochim. Cosmochim. Acta* **68**, 2799–2814.

Kukkadapu, R.K., Zachara, J.M., Fredrickson, J.K., Kennedy, D.W., Dohnalkova, A.C., McCready, D.E., 2005. Ferrous hydroxy carbonate is a stable transformation product of biogenic magnetite. *Am. Mineral.* **90**, 510–515.

Liger, E., Charlet, L., Van Cappellen, P., 1999. Surface catalysis of uranium(VI) reduction by Fe(II). *Geochim. Cosmochim. Acta* **63**, 2939–2955.

Liu, C.G., Zachara, J.M., Gorby, Y.A., Szecsody, J.E., Brown, C.F., 2001. Microbial reduction of Fe(III) and sorption/precipitation of Fe(II) on *Shewanella putrefaciens* strain CN32. *Environ. Sci. Technol.* **35**, 1385–1393.

Loyaux-Lawniczak, S., Refait, P., Ehrhardt, J.-J., Lecomte, P., Génin, J.-M.R., 2000. Trapping of Cr by formation of ferrihydrite during the reduction of chromate ions by Fe(II)–Fe(III) hydoxysalt green rusts. *Environ. Sci. Technol.* **34**, 438–443.

Lovley, D.R., 1991. Dissimilatory Fe(III) and Mn(IV) reduction. *Microbial. Rev.* **55**, 259–287.

Lovley, D.R., 1993. Dissimilatory metal reduction. *Ann. Rev. Microbiol.* **47**, 263–290.

Lovley, D.R., Phillips, E.J.P., 1986. Availability of ferric iron for microbial reduction in bottom sediments of the freshwater tidal Potomac River. *Appl. Environ. Microbiol.* **52**, 751–757.

Mehra, O.P., Jackson, M.L., 1960. Iron oxides removed from soils and clays by a dithionite–citrate system buffered with sodium bicarbonate. *Clays Clay Miner.* **7**, 317–327.

Moore, D.M., Reynolds Jr., R.C., 1997. *X-ray Diffraction and the Identification and Analysis of Clay Minerals*. Oxford University Press, Oxford/New York.

Murad, E., Cashion, J., 2004. *Mössbauer Spectroscopy of Environmental Materials and Their Industrial Utilization*. Kluwer Academic Publishers, (Boston, Dordrecht, New York, London).

Nealson, K., Saffarini, D., 1994. Iron and manganese in anaerobic respiration: environmental significance, physiology, and regulation. *Ann. Rev. Microbiol.* **48**, 311–343.

Nevin, K.P., Lovley, D.R., 2000. Potential for nonenzymatic reduction of Fe(III) via electron shuttling in subsurface sediments. *Environ. Sci. Technol.* **34**, 2472–2478.

Newman, D.K., Kolter, R., 2000. A role for excreted quinones in extracellular electron transfer. *Nature* **405**, 94–97.

North, N.N., Dollhopf, S.L., Petrie, L., Istok, J.D., Balkwill, D.L., Kostka, J.E., 2004. Change in bacterial community structure during in situ biostimulation of subsurface sediment cocontaminated with uranium and nitrate. *Appl. Environ. Microbiol.* **70**, 4911–4920.

O'Loughlin, E.J., Kelly, S.D., Cook, R.E., Csencsits, R., Kemner, K.M., 2003. Reduction of uranium(VI) by mixed iron(II)/iron(III) hydroxide (green rust): formation of UO_2 nanoparticles. *Environ. Sci. Technol.* **4**, 721–727.

Ona-Nguema, G., Abdelmoula, M., Jorand, F., Benali, O., Géhin, A., Block, J-C., Génin, J.-M.R., 2002. Iron (II,III) hydroxycarbonate green rust formation and stabilization from lepidocrocite bioreduction. *Geochim. Cosmochim. Acta* **36**, 16–20.

Peacock, A.D., Chang, Y.-J., Istok, J.D., Krumholz, L., Geyer, R., Kinsall, B., Watson, D., Sublette, K.L., White, D.C., 2004. Utilization of microbial biofilms as monitors of bioremediation. *Microb. Ecol.* **47**, 284–292.

Pecher, K., Haderlein, S.B., Schwarzenbach, R.P., 2002. Reduction of polyhalogenated methanes by surface-bound Fe(II) in aqueous suspension of iron-oxides. *Environ. Sci. Technol.* **36**, 1734–1741.

Peretyazhko, T., Sposito, G., 2005. Iron(III) reduction and phosphorus solubilization in humid tropical forest soils. *Geochim. Cosmochim. Acta* **69**, 3643–3652.

Rancourt, D.G., Ping, J.Y., 1991. Voigt-based methods for arbitrary-shape static hyperfine parameter distributions in Mössbauer spectroscopy. *Nucl. Instrum. Meth. Phy. Rev.* **B58**, 85–87.

Rancourt, D.G., Thibault, P.-J., Mavrocordatos, D., Lamarche, G., 2005. Hydrous ferric oxide precipitation in the presence of nonmetabolizing bacteria: constraints on the mechanism of a biotic effect. *Geochim. Cosmochim. Acta* **69**, 553–577.

Roden, E.E., Zachara, J.M., 1996. Microbial reduction of crystalline Fe(III) oxides: influence of oxide surface area and potential for cell growth. *Environ. Sci. Technol.* **30**, 1618–1628.

Roden, E.E., 2004. Analysis of long-term bacterial vs. chemical Fe(III) oxide reduction kinetics. *Geochim. Cosmochim. Acta* **68**, 3205–3216.

Russell, P.R., Montano, P.A., 1978. Magnetic hyperfine parameters of iron containing minerals in coals. *J. Appl. Phys.* **49**, 1573–1574.

Seabaugh, J.L., Dong, H., Kukkadapu, R.K., Eberl, D.E., Morton, J.P., Kim, J., 2006. Microbial reduction of Fe(III) in the Fithian and Muloorina illites: contrasting extents and rates of bioreduction. *Clays Clay Miner.* **54**, 69–81.

Schwertmann, U., 1959. Die fraktionierte Extraktion der freien Eisenoxyde in Böden, ihre mineralogischen Formen und ihre Entstehyngwweisen (in German). *Z. Pflanzenernähr. Dünger Bodenk.* **84**, 194–204.

Schwertmann, U., Fischer, W.R., 1973. Natural "amorphous" ferric hydroxide. *Geoderma* **10**, 237–247.

Stookey, L.L., 1970. Ferrozine—a new spectrophotometric reagent for iron. *Anal. Chem.* **42**, 779–781.

Van der Zee, C., Roberts, D.R., Rancourt, D.G., Slomp, C.P., 2003. Nanogoethite is the dominant reactive oxyhydroxides phase in lake and marine sediments. *Geology* **31**, 993–996.

Wade, M.L., Agresti, D.G., Wdowiak, T.J., Armendarez, L., 1999. A Mössbauer investigation of iron-rich terrestrial hydrothermal vent systems: lessons for Mars exploration. *J. Geophys. Res.* **104**, 8489–8507.

Wagner, U., Knorr, W., Forster, A., Murad, E., Salazar, R., Wagner, F.E., 1988. Mössbauer study of illite associated with iron oxyhydroxides. *Hyperfine Interact.* **41**, 855–858.

Williams, A.G.B., Scherer, M.M., 2001. Kinetics of Cr(VI) reduction by carbonate green rust. *Environ. Sci. Technol.* **35**, 3488–3494.

Williams, A.G., Gregory, K.B., Parkin, G.F., Scherer, M.M., 2005. Hexahydro-1,3,5-trinitro-1,3,5-triazine transformation by biologically reduced ferrihydrite: evolution of Fe mineralogy, surface area, and reaction rates. *Environ. Sci. Technol.* **39**, 5183–5189.

Zachara, J.M., Fredrickson, J.K., Li, S.W., Kennedy, D.W., Smith, S.C., Gassman, P.L., 1998. Bacterial reduction of crystalline Fe(III) oxides in single phase suspensions and subsurface materials. *Am. Mineral.* **83**, 1426–1443.

Zachara, J.M., Kukkadapu, R.K., Fredrickson, J.K., Gorby, Y.A., Smith, S.C., 2002. Biomineralization of poorly crystalline Fe(III) oxides by dissimilatory metal reducing bacteria (DMRB). *Geomicrobiol. J.* **19**, 179–207.

Zachara, J.M., Kukkadapu, R.K., Gassman, P.L., Dohnalkova, A., Fredrickson, J.K., Anderson, T., 2004. Biogeochemical transformation of Fe minerals in a petroleum-contaminated aquifer. *Geochim. Cosmochim. Acta* **68**, 1791–1805.